Available online at www.sciencedirect.com
ScienceDirect
International Journal of Heat and Mass Transfer 50 (2007) 4891–4900
International Journal of HEAT and MASS TRANSFER
www.elsevier.com/locate/ijhmt

Numerical simulation of conjugate heat and mass transfer during multi-dimensional freeze drying of slab-shaped food products

Jin Hyun Nam [a], Chi Sung Song [b,*]

[a] School of Mechanical and Automotive Engineering, Kookmin University, 861-1 Jeongneung-dong, Seongbuk-gu, Seoul 136-702, Republic of Korea
[b] Korea Institute of Machinery and Materials, 171 Jang-dong, Yusong-gu, Daejeon 305-343, Republic of Korea

Received 30 September 2005; received in revised form 6 November 2006
Available online 29 August 2007

Abstract

The freeze drying characteristics of planar and slab-shaped food products were numerically studied using a simulation program that considered the conjugate heat and mass transfer, sublimation of ice, and motion of sublimation interface. The fixed grid method, which was adopted in the numerical simulation, was able to handle the complex sublimation interface during the multi-dimensional freeze drying of slab-shaped products appropriately. The results showed that the lateral permeable surface of the slab-shaped products significantly altered the freeze drying characteristics by reducing the diffusion length for the water vapor transport as well as by increasing the interfacial area for sublimation. These two effects were found to cooperatively enhance the freeze drying rate while decreasing the average sublimation temperature.

Keywords: Freeze drying; Sublimation; Finite volume method; Fixed grid method

1. Introduction

Freeze drying utilizes sublimation of ice as its main drying mechanism; this differentiates the process from the conventional drying methods that rely on the capillary motion and evaporation of liquid water for drying. In freeze drying, the moisture in products is spatially fixed in the pre-freezing stage, and it is then removed by sublimation of ice in the primary drying stage. To improve the long-term stability of the dried products, the residual water after the primary drying stage may further be reduced by desorption in the secondary drying stage.

Low temperature and pressure below the triple point of water renders excellent quality to the freeze dried products; the most notable advantages of freeze drying are the preservation of the intrinsic microscale structure or the formation of high porosity, minimization of thermal and chemical degradation, retention of volatile or aromatic components, etc. Thus, freeze drying is generally accepted as the best method to dehydrate high quality and heat sensitive products such as quality foods, pharmaceuticals, and biomedical products [1–3].

Despite its merit with respect to quality, freeze drying generally results in low productivity due to long drying time and high operation cost. In pharmaceutical fields, the quality of the final dried products has utmost importance; therefore, researchers have attempted to find optimal operation policies that result in the shortest drying time while satisfying all the quality requirements [4–7]. However, in the food processing fields, alternative freeze drying methods, e.g., atmospheric or microwave freeze drying, have been mainly studied to enhance the process productivity without severe loss in the product quality [8–14]. In any case, a reliable simulation can be a useful tool for the prediction and optimization of freeze drying by reduc-

* Corresponding author. Tel.: +82 42 868 7372; fax: +82 42 868 7355.
E-mail address: scs1675@kimm.re.kr (C.S. Song).

0017-9310/$ - see front matter © 2007 Elsevier Ltd. All rights reserved.
doi:10.1016/j.ijheatmasstransfer.2007.08.004

Nomenclature

c_p	specific heat (J/kg K)
K_D	Darcy flow permeability in dried product (m^2)
D_{eff}	effective vapor diffusivity in dried product (m^2/s)
k	thermal conductivity (W/m K)
h_f	overall heat transfer coefficient at the bottom of the tray (W/m^2 K)
h	height of product (m)
l	width of product (m)
l_s	spacing between products (m)
M_w	molecular mass of water (0.018 kg/mol)
M_{water}	residual water content in product (g)
$\mathbf{m}_w$	mass flux of water vapor (kg/m^2 s)
P_w	vapor pressure (Pa)
$P_w^{sat}(T)$	saturation vapor pressure of water (Pa)
$\mathbf{q}$	heat flux (W/m^2)
R_g	universal gas constant (8.314 J/mol K)
S	ice saturation
T	temperature (K)
$T_{s,avg}$	average sublimation temperature (K)
t	time (s)
x, z	coordinate (m)

Greek symbols

ε	porosity
Δh_s	heat of sublimation of ice (2,821,500 J/kg)
μ	viscosity (kg/m s)
ρ	density (kg/m^3)
σ	Stefan–Boltzmann constant (5.67×10^{-8} W/m^2 K^4)

Superscript

o	old value at the previous time step

Subscripts

0	initial value
ch	drying chamber
hp	heating plate
I	ice
M	matrix
s	sublimation
w	water vapor

ing the trial-and-error time and the cost required for the experimental optimization procedures.

Many food products are freeze dried in slab- or cube-shaped forms; however, there are few numerical models that consider the multi-dimensional heat and mass transfer effect during the freeze drying of food products with such geometries. Difficulties arise in the treatment of the evolution of the complex sublimation interface during the freeze drying of slab-shaped products. Moving grid methods based on the explicit tracking of the interface position and the exact imposition of the interfacial conditions are believed to be the most suitable for dealing with the freeze drying problems. In fact, the multi-dimensional freeze drying problems with a relatively planar sublimation interface, e.g., freeze drying of solutions in vials, were successfully solved by the moving grid methods [5,7,15–17]. However, using the moving grid methods for the freeze drying simulation of the slab-shaped products requires very cumbersome work to handle the complex interface shapes in an appropriate manner. In this case, the fixed grid methods can provide a simpler approach to the multi-dimensional freeze drying problems, although they are believed to be less accurate than the moving grid methods.

Recently, we developed a fixed grid method for the multi-dimensional freeze drying of skim milk solutions and tested its accuracy and efficiency [18]. The fixed grid method produced results that were comparable to those obtained by the moving grid method. However, the fixed grid method required more computation time than the moving grid method because more grid points were used to ensure accuracy. In this study, a fixed grid method was developed to predict the multi-dimensional freeze drying of the slab-shaped food products based on our previous numerical framework [18]. The sublimation–condensation model for the food products [11–14] was adopted to describe the dynamic behavior of the food products during the primary drying stage.

2. Physical model

Conjugate heat and mass transfer during the freeze drying of food products is shown in Fig. 1, where the planar and slab-shaped products are illustrated. In Fig. 1, each product is divided into two regions, a dried region (white) and a frozen region (gray), by the sublimation interface (dashed line). The dried region denotes the region where

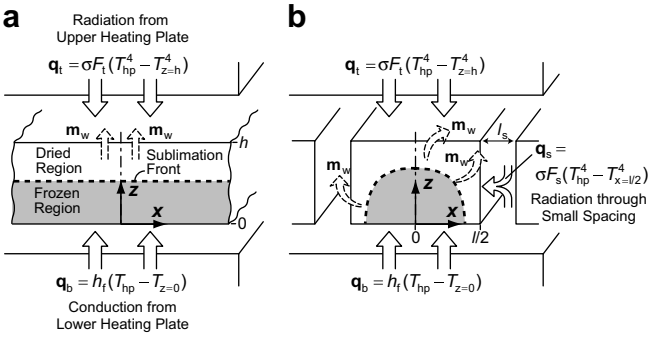

Fig. 1. Conjugate heat and mass transfer during the freeze drying of food products: (a) a planar product and (b) a slab-shaped product.

the sublimation of ice has been completed and the frozen region denotes the region where ice still remains.

During the primary drying stage, moisture (or ice) in the planar product sublimates primarily at the sublimation interface under vacuum pressure, and the resulting water vapor $\mathbf{m}_w$ diffuses through the pores to exit the product. The required energy for the sublimation is provided by conduction through the bottom surface from the lower heating plate $\mathbf{q}_b$ and radiation through the top surface from the upper heating plate $\mathbf{q}_t$.

The freeze drying characteristics of slab-shaped product shown in Fig. 1b are different from those of the planar product in Fig. 1a. This is because the lateral surface of the slab-shaped product is open to the drying chamber and thus allows the transport of water vapor (permeable). Furthermore, the radiation through the lateral surface from the heating plates $\mathbf{q}_s$ also contributes to the difference. Thus, the sublimation interface readily forms beneath the top surface and beside the lateral surface of the slab-shaped product and subsequently moves towards the interior of the product. The uniformly retreating ice front (URIF) assumption, which is valid for freeze drying with a planar sublimation interface, cannot be applied to the slab-shaped product and thus multi-dimensional analysis is required.

3. Mathematical formulation

3.1. Ice saturation

An example of the fixed grid is illustrated in Fig. 2, where the calculation domain is divided into many volume cells for finite volume discretization. The ice content in a volume cell ΔV is quantified by ice saturation S, which is defined as the fraction of pore volume ΔV_P occupied by the ice volume ΔV_I:

$$S = \frac{\Delta V_I}{\Delta V_P} = \frac{\Delta V_I/\Delta V}{\Delta V_P/\Delta V} = \frac{\varepsilon_I}{\varepsilon}, \tag{1}$$

where ε and ε_I denote the porosity and the fraction of the ice volume to the total volume, respectively.

The volume cells in Fig. 2 are categorized as dried cells, frozen cells, and sublimation cells. The physical condition of a volume cell can be determined from the distribution of ice saturation S. The zero ice saturation of a volume cell implies that the cell is a dried cell without ice. Similarly, the volume cells with $S > 0$ are assumed to be frozen cells if they do not contact with the dried cells or the boundary cells that are open to the drying chamber. The sublimation cells, where the sublimation interface exists, satisfy $S > 0$ and at the same time are in contact with the dried cells or are open to the drying chamber.

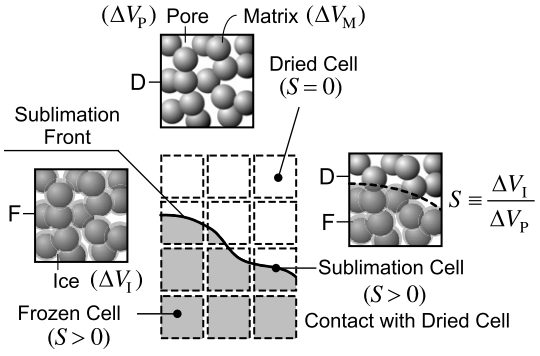

Fig. 2. An exemplary fixed grid for freeze drying simulations.

A simplified microstructural view of the food products is shown in Fig. 2, where the food product is represented as a random packing of spherical particles (termed as matrix) with moisture in the pore space among the particles. In general, the moisture in the food products does not completely fill the pore space (partially saturated) and thus a small mass transfer through the frozen region is always possible. This is believed to contribute to the internal redistribution of moisture in the presence of a temperature gradient.

3.2. Volume-averaged properties

The fixed grid method is based on a single set of governing equations applicable to all the volume cells in the calculation domain. Thus, the volume-averaged properties should be defined in order to consider the variation of the thermo-physical properties according to the ice saturation. The volume-averaged density is defined as

$$\rho = (1-\varepsilon)\rho_M + \varepsilon S \rho_I, \tag{2}$$

where ρ_M and ρ_I are the densities of the matrix and ice, respectively. When $S = 0$, Eq. (2) yields the density of dried product as $\rho_D = (1-\varepsilon)\rho_M$.

The volume-averaged sensible heat capacity is defined as

$$\rho c_p = (1-\varepsilon)\rho_M c_{pM} + \varepsilon S \rho_I c_{pI}, \tag{3}$$

where c_{pM} and c_{pI} are the specific heats of the matrix and ice, respectively.

The volume-averaged thermal conductivity is also defined as a function of ice saturation S:

$$k = (1-\varepsilon)k_M + \varepsilon S k_I + \varepsilon(1-S)k_w, \tag{4}$$

where k_M, k_I, and k_w are the thermal conductivities of the matrix, ice, and water vapor, respectively. When $S = 0$, Eq. (4) results in the thermal conductivity of the dried product as $k_D = (1-\varepsilon)k_M + \varepsilon k_w$.

3.3. Conservation of mass

The conservation of water vapor in a volume cell ΔV yields the following discretized governing equation:

$$\varepsilon \frac{(1-S)\rho_w - (1-S^o)\rho_w^o}{\Delta t}\Delta V + \sum_{j=e,w,n,s} (\mathbf{m}_w)_j \cdot \mathbf{A}_j = -\varepsilon \rho_I \frac{S - S^o}{\Delta t}\Delta V, \tag{5}$$

where the density of water vapor ρ_w can be accurately determined by the ideal gas law (in vacuum pressure):

$$\rho_w = \frac{M_w}{R_g}\frac{P_w}{T}. \quad (6)$$

The subscript j in Eq. (5) denotes the control surfaces that comprise a volume cell (east, west, north, and south faces), and $(\mathbf{m}_w)_j$ and $\mathbf{A}_j$ denote the vapor flux and the outward normal vector of the control surface j. Then, $\sum(\mathbf{m}_w)\cdot\mathbf{A}_j$ is the sum of the water vapor flowing out of the cell or the volume-integrated divergence of the vapor flux. The last term in Eq. (5) denotes the water vapor generation by the sublimation of ice.

A constitutive equation for the vapor flux $\mathbf{m}_w$, required for the mass conservation equations of Eq. (5), is obtained by considering the parallel diffusion and flow through the porous products:

$$\mathbf{m}_w = -(1-S)\frac{M_w}{R_g T}\left[D_{eff} + P_w\frac{K_D}{\mu_w}\right]\nabla P_w, \quad (7)$$

where D_{eff} and K_D denote the effective diffusivity and Darcy permeability [19,20], respectively, in the fully dried products. The term $(1-S)$ is the relative diffusivity or relative permeability, which is included to correct the vapor flux as a function of the ice saturation [11,12].

Due to the large ice/pore interfacial area in the microstructure of the food products, the frozen and sublimation cells can be assumed to be at their thermodynamic equilibrium states; the vapor pressures in those cells are the same as the saturation vapor pressure $P_w^{sat}(T)$. In summary, the governing equation for the vapor pressure is solved only for the dried cells using Eq. (5) with $S = 0$:

$$\varepsilon\frac{\rho_w - \rho_w^o}{\Delta t}\Delta V + \sum_{j=e,w,n,s}(\mathbf{m}_w)_j\cdot\mathbf{A}_j = 0 \quad \text{for dried cells}, \quad (8)$$

while the frozen and sublimation cells are treated as Dirichlet boundaries for the calculation of vapor pressure:

$$P_w = P_w^{sat}(T) \quad \text{for frozen and sublimation cells}. \quad (9)$$

The mass conservation equation of Eq. (5) serves as the governing equation for the evolution of S for the frozen and sublimation cells. The water vapor generated in the frozen and sublimation cells is stored in the pore space or transported out of the cells by diffusion and flow. Then, the rate of reduction of S in a volume cell is equated with the sum of the change in the water vapor contained in that cell, which is the first term on the left hand side of Eq. (5), and the vapor flow out of that cell, which is the second term on the left hand side of Eq. (5).

3.4. Conservation of energy

Consider a volume cell ΔV that experiences sublimation of ice; its ice saturation changes from S^o to S and its temperature changes from T^o to T during a time interval of Δt. The energy conservation equation for that volume cell is

$$\frac{(\rho h) - (\rho h)^o}{\Delta t}\Delta V + \sum_{j=e,w,n,s}\mathbf{q}_j\cdot\mathbf{A}_j = 0, \quad (10)$$

where $\mathbf{q}_j$ denotes the heat flux through the control surface j. The energy contents $(\rho h)^o$ and (ρh) are written as

$$(\rho h)^o = (1-\varepsilon)\rho_M c_{pM}T^o + \varepsilon S^o\rho_I c_{pI}T^o = (\rho c_p)^o T^o, \quad (11a)$$

$$(\rho h) = (1-\varepsilon)\rho_M c_{pM}T + \varepsilon S\rho_I c_{pI}T + \varepsilon(S^o - S)\rho_I(c_{pI}T + \Delta h_s) = (\rho c_p)^o T + \varepsilon(S^o - S)\rho_I\Delta h_s. \quad (11b)$$

Note that $\varepsilon(S^o - S)\rho_I(c_{pI}T + \Delta h_s)$ in Eq. (11b) is the enthalpy of the water vapor that enters or exits upon sublimation. Combining Eqs. (10) and (11) yields the governing equation for temperature (neglecting the convective heat transfer):

$$(\rho c_p)^o\frac{T - T^o}{\Delta t}\Delta V + \sum_{j=e,w,n,s}(-k\nabla T)_j\cdot\mathbf{A}_j = \varepsilon\rho_I\Delta h_s\frac{S - S^o}{\Delta t}\Delta V, \quad (12)$$

where the last term is the latent heat source due to the sublimation of ice; the energy is consumed when ice saturation decreases ($S < S^o$) by the sublimation of ice into vapor. Eq. (12) is also valid when the water vapor enters the volume cell to sublimate into ice ($S > S^o$).

3.5. Boundary conditions

The temperature boundary conditions for the top, bottom, and lateral surfaces of the products are

$$q_t = \sigma F_t\left(T_{hp}^4 - T_{z=h}^4\right) \quad \text{for top surface}, \quad (13a)$$

$$q_b = h_f\left(T_{hp} - T_{z=0}\right) \quad \text{for bottom surface}, \quad (13b)$$

$$q_s = \sigma F_s\left(T_{hp}^4 - T_{x=l/2}^4\right) \quad \text{for lateral surface}, \quad (13c)$$

where F_t is the radiation shape factor for the top surface with respect to the upper heating plates (assumed as 1.0); h_f, the overall heat transfer coefficient for the bottom surface due to the direct contact with the lower heating plate; and T_{hp}, the temperature of the heating plates. There also exists a small radiation heat flux from the upper and lower heating plates towards the lateral surface of the slab-shaped products. Considering the height h of the products and the spacing distance l_s between them, the radiation shape factor of the lateral surface F_s can be determined using the string rule [21] as

$$F_s = \frac{h + l_s - \sqrt{h^2 + l_s^2}}{h} = 1 + \frac{l_s}{h} - \sqrt{1 + \left(\frac{l_s}{h}\right)^2}. \quad (14)$$

The pressure boundary conditions for the surfaces are

$$P_w = P_{w,ch} \quad \text{for surfaces open to the drying chamber}, \quad (15a)$$

$$\mathbf{m}_w = 0 \quad \text{for impermeable surfaces (walls)}. \quad (15b)$$

In addition to the above, all variables are assumed to be uniform at the beginning of the freeze drying ($t = 0$), i.e.,

$$T = T_0, \quad P_w = P_{w0}, \quad S = S_0. \quad (16)$$

3.6. Numerical procedure

The transient calculation for a time step begins with the domain definition procedure, which tags all the volume cells as the dried, frozen, and sublimation cells according to their ice saturations. After the updating the time and variables, the distribution of the temperature T is obtained by solving the energy conservation equation of Eq. (12); the distribution of the vapor pressure P_w is then obtained by solving the mass conservation equation of Eq. (8) for the dried cells with the local thermodynamic equilibrium assumption of Eq. (9) for the frozen and sublimation cells. Once the temperature and vapor pressure is tentatively determined, the evolution of ice saturation S in the frozen and sublimation cells is calculated using the mass conservation equation of Eq. (5). The above calculation is repeated until all the variables converge to a given level of accuracy (1×10^{-3} K for T, 1×10^{-3} Pa for, and 1×10^{-6} for S).

Note that the domain definition procedure is performed only once before the iterative calculation for a time step starts. If the ice saturation in a sublimation cell is initially very small, then it may become smaller than zero during the iterative calculation. However, such negative ice saturation does not deteriorate the accuracy of the calculation because the energy conservation equation of Eq. (12) is arranged in terms of $(\rho c_p)^o$, which is a function of S^o whose value is always positive. Upon exiting the iterative calculation loop, the negative ice saturations in volume cells are distributed to their neighboring volume cells, weighted by the ice saturations of the neighboring cells.

The first-order implicit and second-order central differences were used for the temporal and spatial discretization, respectively. The time step was automatically adjusted for ice saturation in any volume cell not to change more than 0.01 during a time step. The maximum time step was set to 3 s. The discretized algebraic equations for the temperature and vapor pressure were solved with a line-by-line TDMA matrix solver. To handle the non-linear coupling of the temperature, vapor pressure and ice fraction, a successive substitution method with sufficient under-relaxation was used.

4. Results and discussion

Beef has been widely used to study the freeze drying of food products [8–14]. Table 1 lists the selected physical properties of beef from Wang and Shi [11,12]; these properties were derived from Ma and Peltre [8,9], Harper [22], and Perry et al. [23]. The simulated operation conditions are summarized in Table 2. The appropriate size of the volume cells for accurate and efficient calculation was determined first by assessing the simulation results with different grid densities in Fig. 3. The cell size of 0.25 mm (40 volume cells for 1 cm) was found to be sufficient to produce converged results with less than 1% discrepancy.

The histories of the residual water content (for product dimension of $l \times h \times 1$ m), shown in Fig. 3a, indicate that the planar product required 6.41 h to complete drying, while the slab-shaped product required only 5.21 h (about 20% reduction in the drying time). In general, a higher sublimation temperature is required to reduce the drying time (or to increase the drying rate) as it facilitates faster vapor transport by increasing the pressure difference between the sublimation interface and the drying chamber. However, the average sublimation temperature (averaged for all sublimation cells) of the slab-shaped product, shown in Fig. 3b, was always 5–10 °C lower than that of the planar product. This contradictory result of the slab-shaped product (the increase in the drying rate and the decrease in the sublimation temperature) may be explained by the configuration of the sublimation interfaces in Fig. 4.

The interface position is not explicitly tracked during the freeze drying simulation based on the fixed grid method; rather, it is obtained by the post-processing of the results after the simulation. When the ice saturation in a cell becomes half of its initial ice saturation during the simulation, the physical time was recorded as a front time for the volume cell. Then, the sublimation interface configuration shown in Fig. 4 is obtained by contour plotting of the front time distribution.

Fig. 4 shows that the sublimation interface in the slab-shaped product formed just beneath the top surface and

Table 1
Physical properties

Symbol	Value or expression
ρ_I	913 kg/m^3
ρ_M	320 kg/m^3
c_{pI}	2090 J/kg K
c_{pM}	1505 J/kg K
c_{pw}	1866 J/kg K
Δh_s	2,821,500 J/kg
ε	0.75
D_{eff}	$78.5 \times 10^{-4}/(3.4 + P_w/133.3)$ m^2/s
K_D	$4.44 \times 10^{-13} + 3.1589 \times 10^{-12} P_w$ m^2
μ	$0.11 \times (T/273)^{1.5}/(T + 961)$ kg/m s
k_I	2.22 W/m K
k_M	0.20 W/m K
k_w	0.0022 W/m K
$P_w^{sat}(T)$	$R_g T/M_w$ $(0.1 \times \exp(-53.7881 + 0.294552T - 3.987875 \times 10^{-4} T^2))$ Pa

Table 2
Typical operation conditions

Symbol	Value or expression
F_s	0.18
F_t	1.0
h	10 mm
h_f	10 W/m^2 K
l	10 mm
l_s	2 mm
$P_{w,ch}$, P_{w0}	15 Pa
S_0	0.7
T_0	253.15 K
T_{hp}	293.15 K

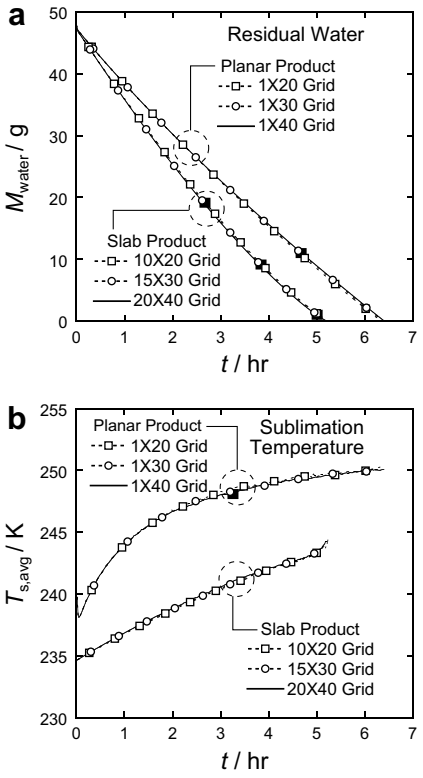

Fig. 3. Histories of (a) residual water content and (b) average sublimation temperature of planar and slab-shaped products during the freeze drying with typical operation conditions.

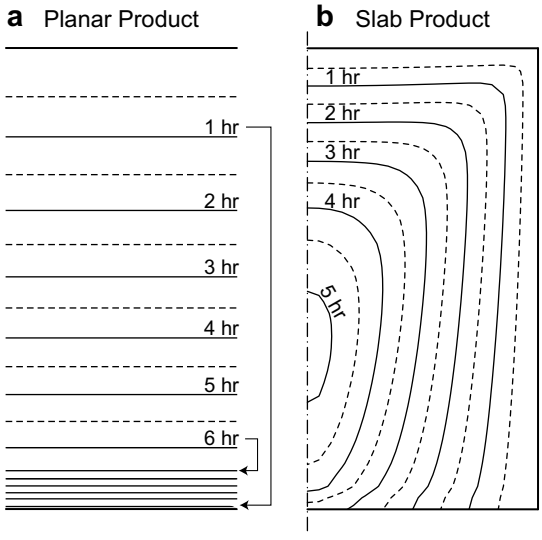

Fig. 4. Predicted sublimation interfaces in (a) planar and (b) slab-shaped products during the freeze drying with typical operation conditions.

near the lateral surface at the beginning of freeze drying and then moved inward. A comparison of Fig. 4a and b clearly shows that the lateral surface of the slab-shaped product significantly altered the overall freeze drying characteristics; they decreased the diffusion length from the sublimation interface to the drying chamber and increased the interfacial area of the sublimation interface. These two effects enabled the shorter drying time with a lower sublimation temperature of the slab-shaped product, observed in Fig. 3. In addition, the primary direction of drying was changed from the axial direction (from top to bottom) for the planar product to the radial direction (from lateral surface to inner core) for the slab-shaped product.

In Fig. 4a, it is observed that a secondary sublimation interface slowly developed near the bottom of the planar product. The two sublimation interfaces were also observed in the numerical studies on microwave freeze drying with a dielectric core by Tao et al. [13] and Wu et al. [14]. The relatively large temperature gradient in the partially saturated frozen region is the main cause for the development of the secondary sublimation interface. However, the secondary sublimation interface is unfavorable for

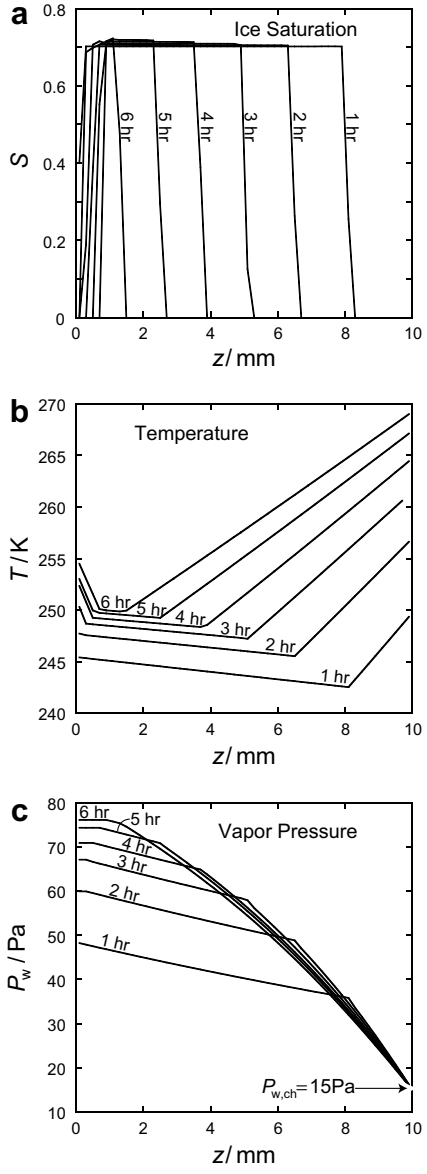

Fig. 5. The distribution of (a) ice saturation, (b) temperature and (c) vapor pressure in a planar product during the freeze drying with typical operation conditions.

productivity because the dried region below the sublimation interface may act as an insulating layer by increasing the heat transfer resistance from the bottom surface towards the sublimation interface.

The freeze drying characteristics of the planar product were investigated in terms of the distribution of ice saturation, temperature, and vapor pressure, as shown in Fig. 5. The distribution of ice saturation shown in Fig. 5a clearly shows the development of the secondary sublimation interface near the bottom of the planar product ($z = 0$ mm). Water vapor sublimated from the secondary sublimation interface was either transported out of the product by diffusion or deposited in the frozen region by resublimation into ice causing a slight increase in the ice saturation. The existence of the secondary sublimation interface is also demonstrated by the three-segmented linear distribution of the temperature and that of vapor pressure, as shown in Fig. 5b and c. The maximum temperature or the maximum vapor pressure is observed to steadily increase with time because of the increased mass transfer resistance according to the thickness of the dried region.

The freeze drying characteristics of slab-shaped product were investigated by the multi-dimensional distribution of ice saturation, temperature, and vapor pressure, as shown in Fig. 6. The ice saturation in the frozen region remained relatively constant around 0.7 ($S_0 = 0.7$), except near the bottom surface where the ice saturation increased slightly over 0.7. The distribution of the temperature and water vapor, shown in Fig. 6b and c, demonstrates that the heat and mass transfer during the freeze drying of slab-shaped products is a fully multi-dimensional process.

The spatial gradient of the temperature in the dried region is considerably larger than that in the frozen region in Fig. 6b; however, the actual heat transfer through the dried region is relatively small because of the small thermal conductivity of the dried region (0.05 W/m K for the dried region and 1.2 W/m K for the frozen region with $S = 0.7$). In Fig. 6c, the spatial gradient of the vapor pressure in the

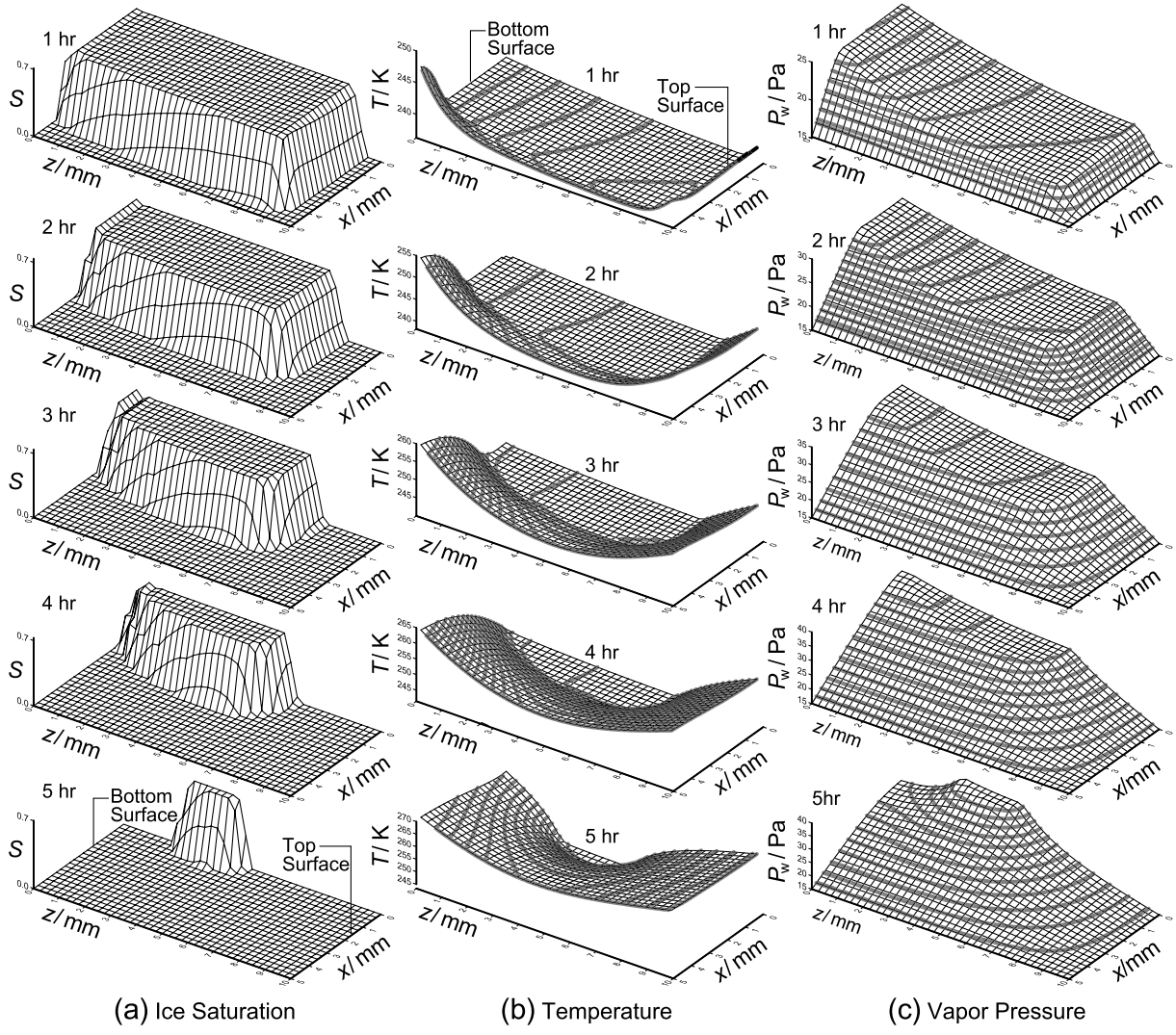

Fig. 6. The distribution of (a) ice saturation, (b) temperature and (c) vapor pressure in a slab-shaped product during the freeze drying with typical operation conditions.

frozen region is caused by its temperature gradient as predicted by the saturation vapor pressure $P_w^{sat}(T)$ in Eq. (9). However, due to the small pore space available in the frozen region, the sublimation of ice from the frozen region is not large.

Fig. 7 shows the heat and mass flows through the top, bottom, and lateral surfaces during the freeze drying of the slab-shaped product. The conduction from the lower heating plate is found to be the main source of energy for sublimation. However, the radiation through the top and lateral surfaces is also considerable, contributing about 40% of the total energy transfer. The heat flow through the bottom surface decreases rather rapidly from the initial 2.86 to the final 0.93 J/s; this is attributed to the development of the dried region near the bottom surface.

Fig. 7b indicates that the sublimated water vapor primarily exits the slab-shaped product through the lateral surface, which can be also inferred from the spatial gradient of the vapor pressure shown in Fig. 6c. The initial vapor flow through the lateral surface is about two times larger than that through the top surface, similar to the area ratio of the lateral surface to the top surface ($2h/l$). However, at the end of the freeze drying, almost 80% of the water vapor generated flows through the lateral surface.

The effect of the product geometry on the freeze drying characteristics is investigated by varying the product height h as 5, 10, 15 and 20 mm, as shown in Fig. 8. The rather linear drying curves for the planar products are the result of a relatively constant drying rate. However, the slab-shaped products exhibit more non-linear drying behaviors; the drying rate is high at the beginning but decreases rapidly. The short diffusion length and the large interfacial area for sublimation is the main reason for the initial high drying rate. However, as the freeze drying proceeds, the interfacial area decreases and the frozen region becomes surrounded by the insulating dried region; this leads to a lower drying rate in the latter part of the freeze drying.

Despite the difference in the freeze drying characteristics of the planar and slab-shaped products as shown by Fig. 8a, their drying times for $h = 5$ mm are similar in Fig. 8b but the difference increases as the product height increases. Fig. 8b shows that the drying time of the slab-shaped products is less sensitive to the product height than that of the planar products. Note that the maximum diffusion length for vapor exhaust is h for planar products, while it is $\min(h, l/2)$ for the slab-shaped products. Thus, the slab-shaped products in Figs. 8 and 9 have a constant maximum diffusion length of $l/2$ or 5 mm, while those of the planar products change according to the product height.

Fig. 9 shows that the configuration of the sublimation interfaces during the freeze drying of the slab-shaped prod-

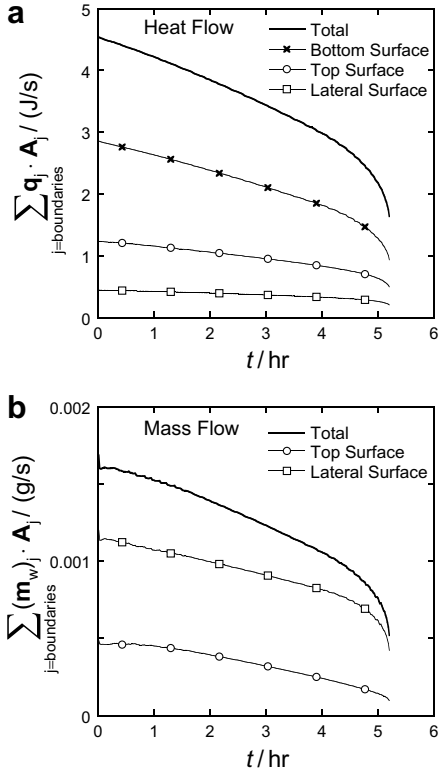

Fig. 7. The rate of (a) heat flow and (b) mass flow through each surface of a slab-shaped product during the freeze drying with typical operation conditions.

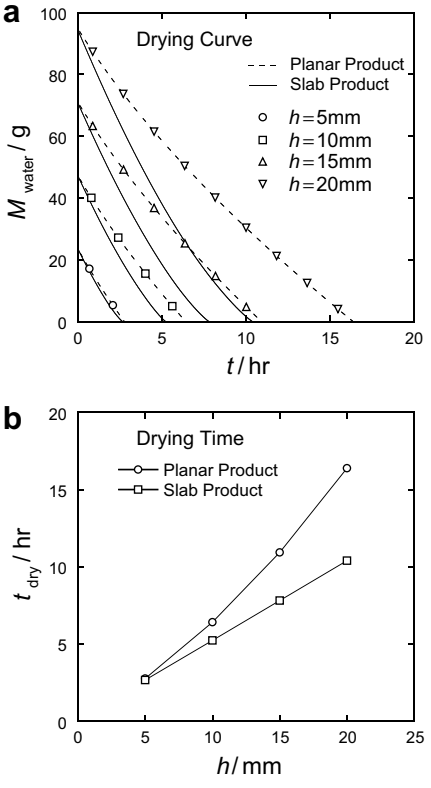

Fig. 8. Effect of product height on (a) drying curves and (b) drying times of planar and slab-shaped products.

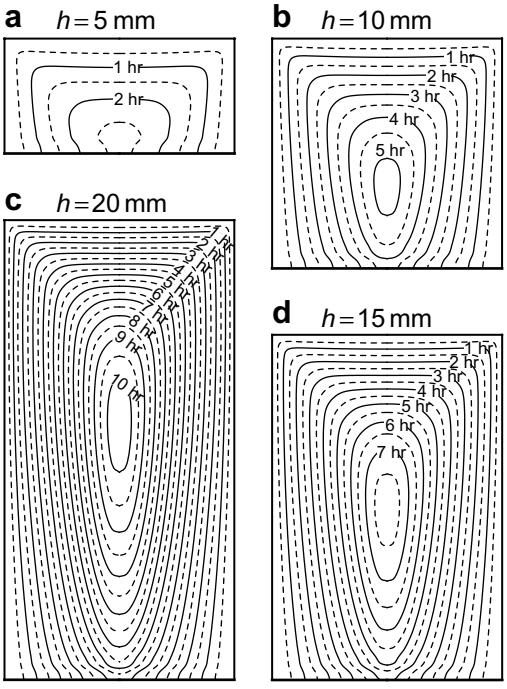

Fig. 9. Predicted sublimation interfaces of slab-shaped products for product height of (a) 5 mm, (b) 10 mm, (c) 15 mm, and (d) 20 mm.

ucts with different product heights. It is observed that the primary direction of drying is the radial direction from the lateral surface to the inner core. The region where freeze drying is completed last moves upward according to the product height, which results in a much lower drying rate due to decreased heat transfer from the bottom surface.

5. Summary

A fixed grid numerical simulation was conducted to investigate the freeze drying characteristics of the planar and slab-shaped food products. The complex sublimation interfaces encountered in the slab-shaped products were well handled by the fixed grid method, demonstrating that the developed numerical framework can be a useful tool for the prediction and optimization of the multi-dimensional freeze drying of food products.

The simulation showed that the lateral surface of the slab-shaped products was favorable for reducing both the drying time and the sublimation temperature by decreasing the diffusion length for vapor transport and increasing the interfacial area for sublimation. The existence of the secondary sublimation interface due to the temperature gradient in the frozen region was also observed during the freeze drying simulation of the planar products. The effects of product height on the freeze drying characteristics were then studied. When the product height was small, the drying times for both the planar and the slab-shaped products were similar. However, as the product heights increased, the freeze drying of the slab-shaped products required a significantly shorter time to complete drying than the freeze drying of the planar products.

Acknowledgement

The first author acknowledges the support from the 2006 research fund of Kookmin University in Korea for publication of this work.

References

[1] M.J. Millman, A.I. Liapis, J.M. Marchello, An analysis of the lyophilization process using a sorption–sublimation model and various operation policies, AIChE J. 31 (1985) 1594–1604.
[2] A.I. Liapis, Freeze drying, in: A.S. Majumdar (Ed.), Handbook of Industrial Drying, Marcel Dekker, New York, 1987, pp. 295–326.
[3] C. Ratti, Hot air and freeze-drying of high-value foods: a review, J. Food Eng. 49 (2001) 311–319.
[4] A.I. Liapis, R.J. Litchfield, Optimal control of a freeze dryer, Chem. Eng. Sci. 34 (1979) 975–981.
[5] P. Sheehan, A.I. Liapis, Modeling of the primary and secondary drying stages of the freeze drying of pharmaceutical products in vials: numerical results obtained from the solution of a dynamic and spatially multi-dimensional lyophilization model for different operation policies, Biotechnol. Bioeng. 60 (1998) 712–728.
[6] H. Sadikoglu, A.I. Liapis, O.K. Crosser, Optimal control of the primary and secondary drying stages of solution freeze drying in trays, Drying Technol. 16 (1998) 399–431.
[7] H. Sadikoglu, M. Ozdemir, M. Seker, Optimal control of the primary drying stage of freeze drying of solutions in vials using variational calculus, Drying Technol. 21 (2003) 1307–1331.
[8] Y.H. Ma, P. Peltre, Freeze dehydration by microwave energy: Part I. Theoretical investigation, AIChE J. 21 (1975) 335–344.
[9] Y.H. Ma, P. Peltre, Freeze dehydration by microwave energy: Part II. Experimental investigation, AIChE J. 21 (1975) 344–350.
[10] T.K. Ang, J.D. Ford, D.C.T. Pei, Microwave freeze-drying of food: a theoretical investigation, Int. J. Heat Mass Transfer 20 (1977) 517–526.
[11] Z.H. Wang, M.H. Shi, Numerical study on sublimation–condensation phenomena during microwave freeze drying, Chem. Eng. Sci. 53 (1998) 3189–3197.
[12] Z.H. Wang, M.H. Shi, The effect of sublimation–condensation region on heat and mass transfer during microwave freeze drying, J. Heat Transfer 120 (1998) 654–660.
[13] H.W. Wu, Z. Tao, G.H. Chen, H.W. Deng, G.Q. Xu, S.T. Ding, Conjugate heat and mass transfer process within porous media with dielectric cores in microwave freeze drying, Chem. Eng. Sci. 59 (2004) 2921–2928.
[14] Z. Tao, H.W. Wu, G.H. Chen, H.W. Deng, Numerical simulation of conjugate heat and mass transfer process within cylindrical porous media with cylindrical dielectric cores in microwave freeze-drying, Int. J. Heat Mass Transfer 48 (2005) 561–572.
[15] W.J. Mascarenhas, H.U. Akay, M.J. Pikal, A computational model for finite element analysis of the freeze-drying process, Comput. Method Appl. Mech. Eng. 148 (1998) 105–124.
[16] C.S. Song, J.H. Nam, C.-J. Kim, S.T. Ro, A finite volume analysis of vacuum freeze drying processes of skim milk solution in trays and vials, Drying Technol. 20 (2002), 20, 283–305.
[17] C.S. Song, J.H. Nam, C.-J. Kim, S.T. Ro, Temperature distribution in a vial during freeze-drying of skim milk, J. Food Eng. 67 (2005) 467–475.
[18] J.H. Nam, C.S. Song, An efficient calculation of multi-dimensional freeze drying problems using fixed grid method, Drying Technol. 23 (2005) 2491–2511.
[19] R.B. Bird, W.E. Stewart, E.N. Lightfoot, Transport Phenomena, second ed., Wiley, New York, 2002, pp. 513–542.

[20] M. Kaviany, Principles of Heat Transfer in Porous Media, second ed., Springer, New York, 1999, pp. 365–390.
[21] H.C. Hottel, Radiant Heat Transmission, in: W.H. McAdams (Ed.), Heat Transmission, third ed., McGraw-Hill, New York, 1954, pp. 55–125.
[22] J.C. Harper, Transport properties of gases in porous media at reduced pressures with reference to freeze drying, AIChE J. 8 (1962) 298–302.
[23] H.R. Perry, D. Green, J.O. Maloney, Perry's Chemical Engineering Handbook, seventh ed., McGraw-Hill, New York, 1997, pp. 2-304–2-306.